中國機械工程學刊第四十四卷第四期第 361~370 頁(民國一百一十二年)
Journal of the Chinese Society of Mechanical Engineers, Vol.44, No.4, pp361~370 (2023)

Capacity Fading of Lithium-Ion Batteries Simulation Based on Multiphysics Coupling

Zhi-Hao Song *, Xin-Tian Liu**, Kang-Feng Qian*,
Bi-Xiong Huang***, Yi-Quan Wang*

Keywords：lithium-ion battery, heat transfer, theory of porous electrodes, stress spectra, multiphysics coupling.

ABSTRACT

For the analysis of the battery life under 1C charging and discharging condition, lithium-ion battery is selected as the research object, the electrochemical simulation model of the battery is constructed based on the theory of porous electrodes. The influence of external stress on the performance of lithium battery is analyzed by using the stress spectrum collected by Lithium-ion battery pack. The 1C charging and discharging condition of the lithium-ion battery is simulated by the electrochemical - Solid heat transfer - fluid heat dissipation - external stress coupling, and the cycle life of the lithium battery is analyzed. A method to reduce the amount of computation is used for the solid electrolyte interphase (SEI) generation reaction, the influence of stress on SEI generation is analyzed.

INTRODUCTION

To meet the energy needs of the electronics and automotive industries, lithium batteries provide a solution of low cost, long cycle life and high energy density (Yu et al., 2020). Lithium battery is the power source of electric vehicle, and its performance directly affects the performance of the whole vehicle (Shang et al., 2019).

Lithium batteries are composed of anode and cathode, separators and electrolyte, etc. If mechanical stress exists, the softer parts of the battery, such as the separators, will have great changes, where the separators have the effect of electronic insulation and conduction Li+ (Yusuf et al.,2020).

The charging and discharging behavior of lithium-ion batteries and the constant expansion of the negative electrode in the long-term cycle exert a certain mechanical pressure on the separator (Cannarella et al., 2014). A method that suppresses the mechanical stress in silicon anode with the control of the upper cut-off voltage for delithiation is proposed (Zhang et al., 2020). A method for fracture problems in bi-layer electrode is developed to analysis the effect of discharging current density on the stress field of bi-layer electrode (Zhang et al., 2020). The diffusion-induced stresses (DIS) generated in a cylindrical composition-gradient electrode is studied by the finite deformation theory and the stress-induced diffusion hypothesis (Zhong et al., 2017). To sum up, in driving condition, the battery of electric vehicle is continuously affected by random external stress, so the influence on external stress could not be ignored.

A rapid rise in the internal temperature of the battery was caused by internal resistance heat, polarization heat release and electrochemical reaction heat (Seaman et al., 2014; Fernandes et al., 2018). A high temperature inside the battery could cause a variety of reactions inside the battery, such as decomposition reaction of SEI (Naseem et al., 2021), reaction of embedded lithium carbon (LixC6) with electrolyte (Zhou et al., 2020), reaction between embedded lithium carbon and binder (Zheng et al., 2019), electrolyte decomposition reaction (Tomai et al., 2018) and decomposition reaction of positive electrode materials (Sharova et al., 2017), these reactions had a great impact on the life of lithium batteries.

The degradation of lithium-ion battery was mainly occurring in two forms: the capacity fading, and an increase in the internal resistance (Kakimoto et al., 2016). The endurance of electric vehicles was affected by the capacity, which was particularly important for the electric vehicles (Reichl et al., 2018). There were many different reasons for the capacity attenuation of lithium batteries, such as the growth of the parasitic solid electrolyte interface (SEI) (Ekstrom et al., 2015), the reduction of the reactive substance (recyclable lithium) involved in the

Paper Received March, 2022. Revised April, 2023. Accepted August, 2023. Author for Correspondence: Xin-Tian Liu.

*   *Student, School of Mechanical and Automotive Engineering, Shanghai University of Engineering Science, Shanghai 201620, China.*

*** Professor, School of Mechanical and Automotive Engineering, Shanghai University of Engineering Science, Shanghai 201620, China.*

reaction (Marques et al., 2019) and the degeneration of the diaphragm (Lagadec et al., 2019).

Many scholars had done the following studies on the attenuation of battery capacity fade. The characteristics of the degradation inconsistency of LIBPs was developed to analyzing the capacity degradation of battery pack (Yang et al., 2019). In order to obtain the optimal operating temperature of the battery, the operating temperature was assumed to be a variety of distributions, and the optimal operating temperature was finally obtained at 25-40 ℃ (Quan et al., 2020). Zheng proposed that the effective capacity loss of the battery pack is the sum of the capacity loss of the minimum charging capacity battery and the difference of the active lithium-ion loss between different batteries (Peng et al., 2019). A simultaneously coupling modeling approach to study the electrochemical and thermal behavior of lithium-ion batteries under large mechanical deformation had been developed (Tian et al., 2021).

To sum up, in order to realize the driving condition simulation of EV under the electrochemical - Solid heat transfer - fluid heat dissipation - external stress coupling, the stress spectrum collected by real vehicle is converted to serve as the input signal of random external stress of lithium battery. At the same time, in order to manage the heat of lithium battery and maintain the system, Simulation of heat dissipation in lithium-ion batteries is carried out (Kupper et al., 2019). Under the above conditions, the attenuation process of battery capacity is analyzed by considering the SEI generation reaction.

ELECTROCHEMICAL REACTION OF LITHIUM BATTERIES

The positive electrode of the battery is LMO electrode, The negative electrode is graphite electrode, The liquid electrolyte is LiPF6.

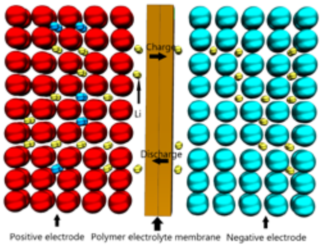

Fig. 1. Electrochemical reaction of lithium battery

The battery model is a one-dimensional model of the battery cross-section which ignores Edge effects on battery length and height (Doyle et al., 1996; Doyle, 1993; Guo et al., 2011; Dao et al., 2012). This model assumes that the electrode active material is a spherical particle with a fixed radius, and carries out modeling on the scale of one dimension for lithium battery, which divides the battery into three parts, namely, negative electrode, diaphragm and positive electrode. The electrochemical reaction model of lithium ion is shown in Figure 1.

Conservation Equation of Matter

In the process of discharge, the mass conservation of lithium battery includes solid phase mass conservation and liquid phase mass conservation. Fick's law is adopted to describe the diffusion process of lithium ion in solid phase lithium (Liu et al., 2020; Weng et al., 2019), as shown in Eq. (1):

$$\frac{\partial c_1}{\partial t}=\frac{D_1^{eff}}{r^2}\left[\frac{\partial}{\partial r}\left(r^2\frac{\partial c_1}{\partial r}\right)\right]=D_1^{eff}\left(\frac{2}{r}\frac{\partial c_1}{\partial r}+\frac{\partial^2 c_1}{\partial r}\right), \qquad (1)$$

$$D_1^{eff}=D_1\varepsilon^{\gamma}\,. \qquad (2)$$

where c is lithium-ion concentration, D is diffusion coefficient, r is reaction interface radius, eff is the correction factor of parameter Bruggeman, t is time.

According to Eq. (2), Bruggeman parameter is corrected, and its correction coefficient is 1.5 (Weiglhofer et al., 1997).

The diffusion process of lithium ion in liquid phase is shown in Eq. (3):

$$\varepsilon_2\frac{dc_2}{dt}+\nabla\left\{D_2^{eff}\nabla c_2\right\}=\frac{3\varepsilon_1 J_{1oc}}{R_i F}\left(1-t_+\right). \qquad (3)$$

where J_{1oc} is local current density, R_i is particle radius, t_+ is ion transference number, F is faraday constant. 1, 2 represent solid and liquid phase separately.

According to Faraday's law, the lithium flux on the surface of spherical active particles is described by Eqs. (4) and (5):

$$\left.\frac{\partial c_1}{\partial r}\right|_{r=0}=0\,, \qquad (4)$$

$$-D_1^{eff}\left.\frac{\partial c_1}{\partial r}\right|_{r=R_i}=\frac{J_{1oc}}{F}\,. \qquad (5)$$

Charge conservation equation

Conservation of charge includes conservation of solid phase charge and conservation of ionic charge in liquid phase. Conservation of electron charge is determined according to Ohm's law and conservation of ionic charge is obtained according to concentrated solution theory, as shown in Eqs. (6) and (7):

$$\nabla\left(-k_1^{eff}\nabla\varphi_1\right)=\frac{3\varepsilon_1 J_{1oc}}{R\ F}\,, \qquad (6)$$

$$\nabla\left\{k_2^{eff}\left[-\nabla\varphi_2+\frac{2RT}{F}\left[1+\frac{\partial\ln f}{\partial\ln c_2}\right]\left(1-t_+\right)\frac{\nabla c_2}{c_2}\right]\right\}=\frac{3\varepsilon_1 J_{1oc}}{R\ F}\,. \qquad (7)$$

where φ_1 is solid phase voltage, φ_2 is electrolyte potential. R is the molar gas constant.

Assuming that no electron charge passes through the separators and the electrode surface, as shown in Eqs. (8) and (9):

$$-k_{1,n}^{eff}\nabla\varphi_1\Big|_{x=L_{neg}}=0\,, \tag{8}$$

$$-k_{1,n}^{eff}\nabla\varphi_1\Big|_{x=L_{neg}+L_{sep}}=0\,. \tag{9}$$

where *L_neg* is the thickness of the anode, *L_sep* is the diaphragm thickness.

Reaction Kinetics

The destocking/imbedding reaction of lithium ions is analyzed by using Butter-Volmer formula, as shown in Eq. (10):

$$J_{1oc}=J_0\left\{\exp\left[\frac{\alpha_a\eta F}{RT}\right]-\exp\left[\frac{-\alpha_a\eta F}{RT}\right]\right\}. \tag{10}$$

where J_0 is initial current density, α_a is reaction conversion coefficient of anode electrode, T is battery temperature, η is over potential, R is molar gas constant.

The exchange current density is a function of the lithium-ion concentration in the solid and liquid phases, as shown in Eq. (11):

$$J_0=F\left(k_c\right)^{\alpha_a}\left(k_a\right)^{\alpha_c}\left(c_{1.\max}-c_{1,surf}\right)^{\alpha_a}\left(c_{1,surf}\right)^{\alpha_c}. \tag{11}$$

where α_c is reaction conversion coefficient of cathode electrode, $c_{1.\max}$ is maximum solid concentration, $c_{1,surf}$ is solid phase lithium-ion surface concentration.

When the current at the electrode -electrolyte interface is 0, it is equilibrium potential, as shown in Eq. (12):

$$U_{surf}=\varphi_1-\varphi_2\,. \tag{12}$$

where U_{surf} is equilibrium potential, φ_1 is solid phase voltage, φ_2 is electrolyte potential.

Electrode potential: When the current at the interface between electrode and electrolyte is not 0, as shown in Eq. (13):

$$\eta=\varphi_1-\varphi_2-U_{surf}\,. \tag{13}$$

The values used are as follows:

Table 1. Parameter list

Model	Negative	Positive	Separate
$c_{initial}[mol/m\wedge 3]$	4205	18925	/
$c_{\max}[mol/m\wedge 3]$	21000	/	/
$T[K]$	298	/	/
R_i [m]	2.50e-6	1.70e-6	/
α_c,α_a	0.5	0.5	/
$F[C/mol]$	96487	/	/
ε_1	0.238	0.43	/
ε_2	0.44	0.4	0.37

COUPLING OF STRESS AND ELECTROCHEMICAL

Preprocessing of Stress Spectrum Signals

In order to shorten the test period, the battery load signals are collected in the typical road conditions of the test yard, and the load spectrum is compiled and applied to the bench test or simulation analysis. A six-component force measurement system is adopted to collect the battery load signals. Typical roads such as cobblestone road, damaged road and resonance road are selected in the test field (Liu et al., 2020; Wang et al., 2018). Figure 2 shows the vertical acceleration-time history signals of battery pack when driving on washboard road.

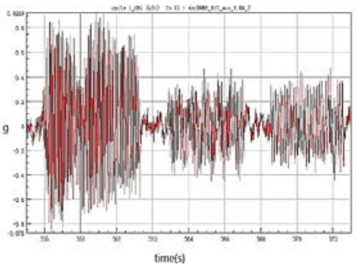

Fig. 2 Battery pack acceleration - Time history

During the load signal collection in the test yard, because of the influence of the performance of the measuring equipment and the surrounding environment, the collected signals may appear abnormal phenomena, such as burr and signal loss. These phenomena can affect the accuracy of the analysis. The collected load signals need to be preprocessed, such as outlier removal and signal denoising. The preprocessing flow of load signal is shown in Figure 3.

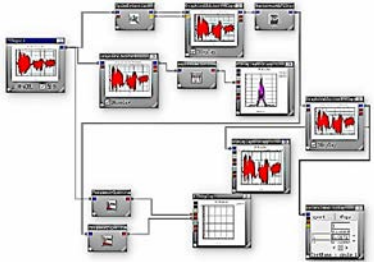

Fig. 3 Preprocessing flow of load signal

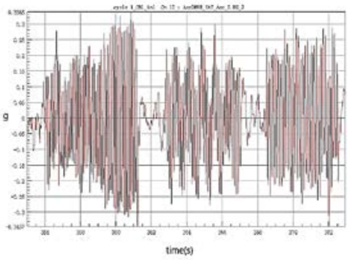

Fig. 4 Preprocessing of load signals

According to the processing process shown in Fig. 3, the pre-processing of the acceleration signal of the battery pack is completed when it is traveling on the washboard road, and the results are shown in Figure 4. The separator is made of polymer material, and the porosity of the diaphragm is changed as a result of pressure changes. In order to consider the influence of pressure on the separator, the separator structure is characterized by interconnected tetrahedra (Sarkar et al., 2019; Dawson et al., 2007; Gioia et al., 2001), as shown in Figure 5.

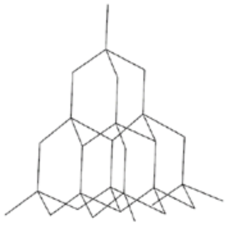

Fig. 5 Separator micromodel

Tetrahedron produces strain due to its compression under pressure. The strain curve can be divided into elastic strain area, plastic strain area and collapse area, which can be described by Eqs. (14), (15) and (16):

$$\varepsilon_i = \frac{\sigma_i}{E}; 0 \le \sigma < \sigma_y \, , \tag{14}$$

$$\varepsilon_i = \frac{\sigma_y}{E} + \frac{\sigma_i - \sigma_y}{H}; \sigma_y \le \sigma < \sigma_d \, , \tag{15}$$

$$\varepsilon_i = \frac{\sigma_y}{E} + \frac{\sigma_d}{H} + \frac{(\sigma_i - \sigma_d)^m}{H_d}; \sigma_i \ge \sigma_d \, . \tag{16}$$

where ε_i is strain, σ_i is stress, σ_y, σ_d is stress boundary, E is elasticity modulus, H is the isotropic hardening coefficient, H_d is the densification hardening coefficient.

The separator strain under pressure affects the diffusion of lithium ions, and the flow model of liquid in foam structure is used to simulate the effect of pressure on the conductivity of lithium ions in the separator.

In the elastic deformation region, the conductivity of lithium ions in the diaphragm is described by Eq. (17):

$$\kappa = \kappa_0 (1 + \varepsilon); 0 \le \varepsilon < \varepsilon_{el} \, . \tag{17}$$

where κ_0 is the conductivity at 0% strain.

In the plastic deformation and collapse zone, the material conductivity is the superposition state of elastic deformation and collapse deformation, and the proportion of elastic deformation χ_{el} and collapse deformation χ_d is expressed by Eqs. (18) and (19):

$$\chi_{el} = \frac{(\varepsilon_d - \varepsilon)(1 - \varepsilon_{el})}{(1 - \varepsilon)(\varepsilon_d - \varepsilon_{el})} \, , \tag{18}$$

$$\chi_d = \frac{(\varepsilon - \varepsilon_{el})(1 - \varepsilon_d)}{(1 - \varepsilon)(\varepsilon_d - \varepsilon_{el})} \, . \tag{19}$$

where $\varepsilon_{el}, \varepsilon_d$ is strain boundary.

Substituting Eqs. (18), (19) into Eq. (17), the conductivity of lithium ions in the plastic deformation zone and collapse deformation zone can be calculated as follow:

$$\kappa = \kappa_1 \frac{(1 + \varepsilon_d)^{2\alpha} (1 + \varepsilon_{el})}{\chi_{el} (1 + \varepsilon_d)^{2\alpha} + \chi_d (1 + \varepsilon_{el})}; \varepsilon_{el} \le \varepsilon < \varepsilon_{\max} \, . \tag{20}$$

where α is an empirical constant.

In the actual driving condition, Eq. (21) is used to convert the acceleration signal into stress after preprocessing the load signal.

$$\sigma = g\rho \, . \tag{21}$$

It can be seen from Fig. 4: $g_{\max} = 0.3385077$, $g_{\min} = -0.3457198$.

According to Eq. (21), the maximum and minimum stress values can be calculated.

On the basis of the stress, the strain of the separator is calculated by Eq. (22):

$$\varepsilon_t = \frac{\sigma_t}{E} \, . \tag{22}$$

Under the driving condition with random external stress, the lithium-ion conductivity of the separator can be known from Eq. (17):

$$\kappa_t = \kappa_2 (1 + \varepsilon_t); 0 \le \varepsilon_t < \varepsilon_{el} \, . \tag{23}$$

where the value of κ_2 comes from the material.

According to Eq. (23), the time-varying conductivity of lithium ions is determined. Cubic spline interpolation is adopted to obtain the change of lithium-ion conductivity in the battery model, as shown in Figure 6:

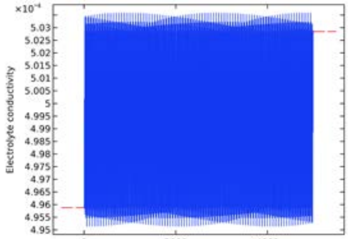

Fig. 6 The conductivity of lithium ions over time

COUPLING OF HEAT

Temperature Derivative

The change in the Gibbs free energy of the reversible battery $\Delta_r G_m$ is described based on the Gibbs Helmholtz equation, as shown in Eq. (24):

$$\Delta_r G_m = \Delta_r H_m + T \left[\frac{\partial (\Delta_r G_m)}{\partial T} \right] . \tag{24}$$

where $\Delta_r G_m$ is Gibbs free energy per mole, $\Delta_r H_m$ is reaction heat.

By substituting $E = \frac{\Delta_r G_m}{zF}$ into Eq. (24), the equation can be rewritten as follow:

$$\Delta_r H_m = zFE - zFT \left[\frac{\partial E}{\partial T} \right]_P \, . \tag{25}$$

where $\left[\frac{\partial E}{\partial T} \right]_P$ is the temperature derivative of battery electromotive force.

Reversible Heat Released for Battery Reaction

The relationship between the Gibbs free energy per mole and the change in molar entropy is as follow:

$$-\Delta_r S_m = \left[\frac{\partial (\Delta_r G_m)}{\partial T} \right]_P = zFT \left[\frac{\partial E}{\partial T} \right]_P \, . \tag{26}$$

where z is the number of charges, $\Delta_r S_m$ reaction of entropy.

Under reversible conditions, the molar reversible heat expression can be expressed as follow:

$$Q_r = T\Delta_r S_m = zFT\left[\frac{\partial E}{\partial T}\right]_P . \quad (27)$$

where Q_r is the molar reversible heat.

When n mol substances participate in reversible heat, the heat produced can be described as follow:

$$Q = nQ_r = zFnT\left[\frac{\partial E}{\partial T}\right]_P . \quad (28)$$

The heat source W can be expressed as:

$$W = \frac{Q}{Vt} = \frac{zFnT\left[\frac{\partial E}{\partial T}\right]_P}{Vt} . \quad (29)$$

Convection Heat Transfer Equation

Heat transfer consists of conduction heat transfer, convection heat transfer and heat radiation (Al-Zareer, 2020). In this paper, convective heat transfer is adopted, as shown in Eq. (30):

$$\rho C_p \frac{\partial T}{\partial t} + \partial C_p u \nabla T + \nabla q = Q + Q_{ted} . \quad (30)$$

where C_p is coefficient of heat transfer, u is the velocity of the flow field, Q_{ted} is thermoelastic damping, ∇q is conduction term.

Table 2. Parameter list

Parameters	Values	Values
L_neg	55e-6[m]	5.5E-5 m
L_sep	30e-6[m]	3E-5 m
L_pos	55e-6[m]	5.5E-5 m
L_neg_cc	7[um]	7E-6 m
L_pos_cc	10[um]	1E-5 m
kT_pos	1.58[W/(m*K)]	1.58 W/(m·K)
kT_neg	1.04[W/(m*K)]	1.04 W/(m·K)
kT_pos_cc	170[W/(m*K)]	170 W/(m·K)
kT_neg_cc	398[W/(m*K)]	398 W/(m·K)
kT_sep	0.344[W/(m*K)]	0.344 W/(m·K)
L_neg	55e-6[m]	5.5E-5 m
L_sep	30e-6[m]	3E-5 m
L_pos	55e-6[m]	5.5E-5 m
r_batt	9[mm]	0.009 m
h_batt	65[mm]	0.065 m
L_neg_cc	7[um]	7E-6 m
L_pos_cc	10[um]	1E-5 m
kT_sep	0.344[W/(m*K)]	0.344 W/(m·K)
L_batt	L_neg+L_neg_cc +L_sep+L_pos+ L_pos_cc	1.57E-4 m

In the normal direction, the thermal conductivity of electrode materials can be expressed as follows:

$$k_r = \frac{\text{L\_batt}}{\text{(L\_pos/kT\_pos+L\_neg/kT\_neg+L\_pos\_cc/kT\_pos\_cc +L\_neg\_cc/kT\_neg\_cc+L\_sep/kT\_sep)}} . \quad (31)$$

In the tangential direction, the thermal conductivity of the electrode material can be expressed as follows:

$$k_t = \frac{\text{(kT\_pos}\cdot\text{L\_pos+kT\_neg}\cdot\text{L\_neg+kT\_pos\_cc}\cdot\text{L\_pos\_cc +kT\_neg\_cc}\cdot\text{L\_neg\_cc+kT\_sep}\cdot\text{L\_sep)}}{\text{L\_batt}} . \quad (32)$$

where k_r is thermal conductivity in the normal direction, k_t is thermal conductivity in the tangential direction, L_sep is the diaphragm thickness, L_pos is the thickness of the anode, L_neg is the thickness of the cathode, kT_pos is thermal conductivity of positive material, kT_neg is thermal conductivity of negative material, kT_sep is thermal conductivity of diaphragm material, kT_pos_cc is positive current collector thermal conductivity, kT_neg_cc is negative current collector thermal conductivity, L_pos_cc is positive current collector thickness, L_neg_cc is negative current collector thickness.

Assuming that the thermal conductivity is related to the position and is little affected by the temperature gradient, the thermal conductivity matrix is diagonal matrix.

CAPACITY FADE THEORY

During the first cycle, the carbon negative electrolyte of lithium-ion battery will form a solid electrolyte film (SEI) on its surface, which is conducive to maintaining the negative structure. The film is composed of lithium carbonate, lithium alkyl ester, lithium hydroxide and other components, as well as some salt decomposers and polymers.

During the formation of SEI membrane, lithium ions in the battery are consumed, resulting in the decrease of battery energy density. The SEI is unstable. During the cycle, the SEI constantly breaks, and the new carbon surface and electrolyte form the new SEI, leading to the continuous loss of lithium ions.

To sum up, based on the parasitic side reaction generated by the SEI on the negative pole (Ramadass et al., 2004; Ning et al., 2006), as shown in Eq. (33):

$$S + Li^{+} + e^{-} \rightarrow P_{SEI} . \quad (33)$$

where S is electrolyte, Li^{+} is Lithium-ion, e^{-} is electronic, P_{SEI} is SEI.

The reaction equation is shown in Eq. (34):

$$i_{1oc,SEI} = -\left(1+HK\right)\frac{Ji_{loc,1C,\ ref}}{\exp\left(\frac{\alpha\eta_{SEI}F}{RT} + \frac{q_{SEI}fJ}{i_{1oc,1C,ref}}\right)} . \quad (34)$$

where $i_{1oc,SEI}$ is local current density of the formation of SEI, HK is dimensionless graphite expansion factor function, $J_{i1oc,SEI}$ is the exchange current density of the formation of SEI, $i_{loc,1C,\ ref}$ is Local current density at 1C discharge rate, α is reaction reduction coefficient of the formation of SEI, η_{SEI} is the over potential of SEI. q_{SEI} is the SEI generated locally accumulated charges, f is lumped dimensionless parameters based on SEI membrane properties, J is dimensionless exchange current density of the formation of SEI.

According to Faraday's law and Eqn. (34), the concentration change of SEI is determined:

$$\frac{\partial c_{SEI}}{\partial t} = -\frac{v_{SEI} i_{loc,SEI}}{nF} . \tag{35}$$

According to Eq. (35), the cumulative charge number is calculated as follows:

$$q_{SEI} = \frac{Fc_{SEI}}{A_v} . \tag{36}$$

where Av is specific surface area of battery.

The film thickness of SEI is the sum of the initial film thickness $\delta_{film,0}$ and the film thickness generated by the reaction. The calculation expression is shown in Eq. (37):

$$\delta_{film} = \frac{c_{SEI}}{A_v \rho_p} + \delta_{film,0} . \tag{37}$$

where δ_{film} is film thickness, $\delta_{film,0}$ is the initial film thickness, ρ_p is product density.

The film resistance is calculated according to the film thickness, as shown in Eq. (38):

$$R_{film} = \frac{\delta_{film}}{\kappa_0} . \tag{38}$$

where R_{film} is film resistance.

residual capacity can be expressed as follow:

$$q_1 = \frac{q_0 - q_{SEI}}{q_0} . \tag{39}$$

where q_0 is initial value.

Table 3. Parameter list

Parameters	Values
H	6.7
f	2.0e2[1/s]
J	8.4e-4
α	0.5
q_0	$c_{\max}(1-0.25) * epss\_pos * L\_pos * F\_const$
K	Table 4.

Table 4. Piecewise K

Piecewise K	Start	End
2	0	0.3
0	0.3	0.7
1	0.7	1

CASE SIMULATION

The geometric model of lithium-ion battery adopts one-dimensional structure. Solid heat transfer model and laminar heat dissipation model adopt three-dimensional structure, and the internal temperature and airflow distribution of the battery pack can be observed. Under the above conditions, one - dimension and three - dimension cross - scale modeling is completed.

Model Definition And Boundary Conditions

(1) Lithium battery

The experimental object is a Korean Samsung INR18650-30Q lithium-ion battery, and the battery pack consists of 32 cells, the detailed parameters are shown in Table 5. Assuming that the electrode active material is composed of spherical particles of fixed radius, the conservation of ionic charge and the conservation of matter were modeled according to the binary 1:1 electrolyte equation. The mass transport in spherical particles is described by Fick's diffusion law and the lithium-ion transport in spherical coordinates is described by diffusion equation. The conservation of charge includes the conservation of solid phase charge and ionic charge in liquid phase, the conservation of electron charge according to Ohm's law, and the conservation of ionic charge according to concentrated solution theory. The Butler-Volmer electrode dynamics formula is used to describe the local charge transfer current density in the electrode, and the conservation of charge and the conservation of matter is introduced as the source term or sink term.

Considering the conservation of electron-induced current, zero potential is set on the fluid collector boundary of the negative pole, current density is specified on the fluid collector boundary of the positive pole, and the internal boundary on both sides of the diaphragm is the insulation boundary. In order to realize the conservation of ionic charge in the electrolyte, the fluid set boundary is insulated, and the flux boundary condition is used for the conservation of matter.

Table 5. INR18650-30Q Single cell specifications

Item	Specification
Nominal voltage	3.6V
Standard charge	CCCV, 1.50A, 4.20 ± 0.05 V, 150mA cut-off
Rated charge	CCCV, 4A, 4.20 ± 0.05 V, 100mA cut-off
Charging time	Standard charge: 180min / 150mA cut-off Rated charge: 70min (at 25°C) / 100mA cut-off
Max. continuous discharge (Continuous)	15A (at 25°C), 60% at 250 cycles
Discharge cut-off voltage End of discharge	2.5V
Cell weight	48.0g max

(2) Heat transfer

Due to the complexity of different length and geometry, lithium battery is characterized by single-layer thickness of tens of microns, length and height direction of tens of centimeters, and is also multi-layer structure. 3D battery model leads to a large amount of computation.

Compared with the generated heat, the thermal conductivity of each part of the lithium battery is higher, the temperature distribution is relatively uniform, and the electrochemical performance is not sensitive to small temperature changes. Model is assumed that the reservoir and the temperature are in equilibrium. The specified boundary temperature (Barbarians-style border) is adopted and a constant temperature boundary is given at the entrance of the flow field.

Time Acceleration Factor

The capacity attenuation of lithium battery is discussed under driving conditions. The difference between each cycle is very small, and obvious capacity attenuation phenomenon can be found after several cycles.

Hypothesis: Each charge-discharge cycle represents the average aging characteristics of a large number of cycles; After a charge and discharge cycle, all lithium captured in the SEI layer comes from the negative pole. According to Eq. (33), the chemical equivalent of reaction generated by SEI is rewritten to optimize the operational speed of capacity fade. The improved SEI generation reaction is shown in Eq. (40):

$$(\tau+1)S + Li^{+} + e^{-} + (\tau-1)Li(s) \rightarrow \tau P_{SEI}\ . \qquad (40)$$

where τ is the time acceleration factor, and represents the actual number of cycles per battery cycle. In this model, τ is 250.

Simulation For Capacity Fade Acceleration

Consider the capacity loss at different C-rate of 0.1C,0.3C,0.7C,1C,2C, respectively, as shown in Figure 7 and Table 6. The capacity loss becomes more severe as the C-rate increases, and the capacity loss with stress is greater than that without stress at the same C-rate. In the actual working condition, the electric vehicle battery pack C-rate is around 1C, so the capacity loss in the 1C case is mainly considered. The time acceleration factor mentioned in 3.2 is adopted, and 1C charge and discharge cycle is performed.

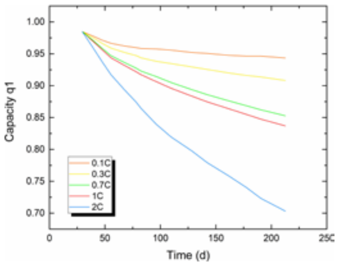

(a)Without stress

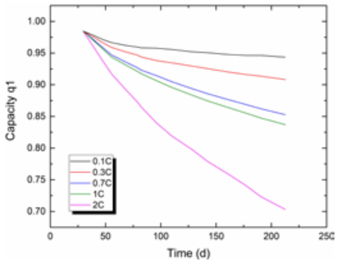

(b)Under stress

Fig. 7 Capacity variation at different C-rate

Table 6. Capacity loss at different C-rate

	Without stress	Under stress
0.1C	4.197%	4.199%
0.3C	7.775%	7.777%
0.7C	13.402%	13.405%
1C	15.009%	15.011%
2C	28.589%	28.591%

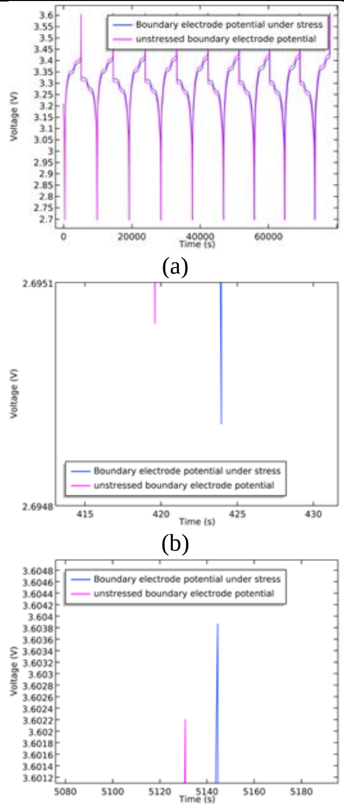

(a)

(b)

(c)

Fig. 8 Voltage variation diagram of the battery

2.7V and 3.6V are the cutoff voltages for lithium-ion batteries, within which batteries should normally operate. As can be seen from Figure 8(a), during charging, the voltage under stress is lower than the unstressed voltage; during discharging, the voltage under stress is higher than the unstressed voltage. As can be seen from Fig. 8(b), (c), The time interval for the first charge without stress is [419.6s,5130.8s], The time interval for the first charge under stress is [424s,5144s], The charging time under stress is longer than that under no stress, and so on in every subsequent cycle.

The SOC obtained from monitoring is shown in Figure 9(a), The time intervals for the first charge under stress and on stress match with Fig. 8(b), (c).

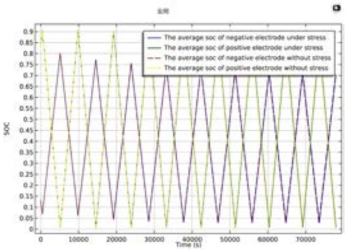

(a)

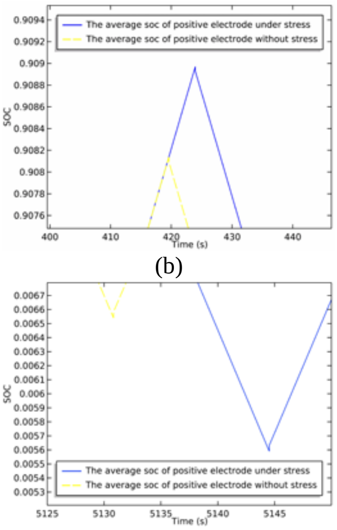

(b)

(c)

Fig. 9 Battery soc and positive and negative SOC changing over time

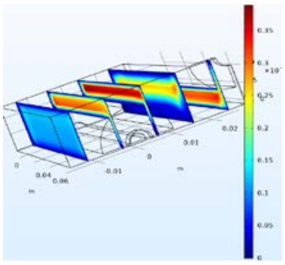

Fig. 10 Speed section in battery pack

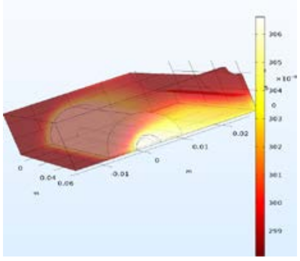

Fig. 11 Temperature distribution of battery pack

Figure 10 and Figure 11 respectively show the distribution diagram of wind speed and temperature inside the battery pack. According to Fig. 11, the outlet temperature is significantly higher than the inlet temperature.

Respectively, Figure 12 and Figure 13 show the relationship between capacity and time and cycle times. The SEI formation reaction occurs during charging, it can be seen from the analysis results of Fig. 8 and 9, The charging time under stress is longer than that under no stress, this results in more lithium ions being consumed when charged under pressure, suggest that capacity is lost even more. As shown in Fig. 12 and 13, the capacity under stress is less than that under no stress because the application of external stress causes a change in the porosity of the diaphragm, which affects the conductivity of lithium ions and thus the ion flux. The ion flux under stress is lower than the ion flux without stress, indicating that stress inhibits ion diffusion, making the capacity lower. Therefore, the capacity under stress is lower than that under no stress due to both the SEI formation reaction and ion flux.

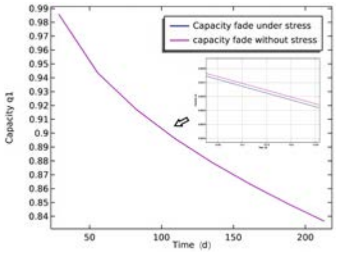

Fig. 12 The attenuation of capacity over time

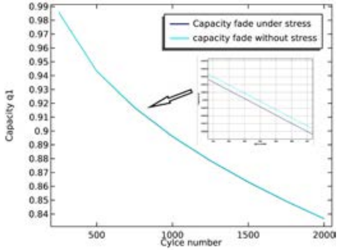

Fig. 13 The capacity decreases for the cycles

CONCLUSIONS

In order to discuss the change of the cycling performance of lithium battery under the influence of temperature and stress in 1C charge and discharge, the change of the performance of lithium battery in long-cycle condition is simulated numerically. The main contents are as follows:

(1) A one-dimensional lithium battery model was established based on the porous electrode theory, and the thermal coupling between the one-dimensional lithium battery model and the three-dimensional battery pack structure was realized by using the assumption of average heat source.

(2) The porous foam was used to simulate the lithium battery separator, referring to the strain curve of typical foam material, the random external stress is transformed into the influence on the conductivity. The separator lithium-ion conductivity under the action of random external stress was determined by using the battery spectrum data of real vehicle.

(3) In the capacity fade simulation process based on SEI generation reaction, in order to solve the problem of long operation time, the equation of SEI generation reaction can be adapted by introducing time acceleration factor to make the SEI generation linearly accumulate, so as to quickly realize the capacity attenuation after multiple charge and discharge cycles, at the same time, the influence of stress on SEI generation reaction is analyzed.

REFERENCES

Al-Zareer, M., “Numerical study of flow and heat transfer performance of 3D-printed Polymer-based battery thermal management,” International Journal of Heat and Mass Transfer, Vol.158, pp.119995 (2020)

Cannarella, J. and Arnold, C.B., “Stress evolution and capacity fade in constrained lithium-ion pouch cells,” Journal of Power Sources, Vol.245, pp.745-751 (2014)

Dao, T.S., Vyasarayani, C.P. and Mcphee, J., “Simplification and order reduction of lithium-ion battery model based on porous-electrode theory,” Journal of Power Sources, Vol.198, pp.329–337 (2012)

Dawson, M.A., Germaine, J.T. and Gibson, L.J., “Permeability of open-cell foams under compressive strain,” International Journal of Solids and Structures, Vol.44, pp.5133-5145 (2007)

Doyle, M., “Modeling of galvanostatic charge and discharge of the lithium/ polymer/ insertion cell,” Journal of the Electrochemical Society, Vol.140, No.6, pp.1526-1533 (1993)

Doyle, M., Newman, J., Gozdz, A.S., Schmutz, C.N. and Tarascon, J.M., “Comparison of modeling predictions with experimental data from plastic lithium-ion cells,” Journal of the Electrochemical Society, Vol.143, No.6, pp.1890-1903 (1996)

Ekstrom, H. and Lindbergh, G., “A model for predicting capacity fade due to SEI formation in a commercial graphite/LiFePO4 cell,” Journal of the Electrochemical Society, Vol.162, No.6, pp.1003-1007 (2015)

Fernandes, Y., Bry, A. and De, P.S., “Identification and quantification of gases emitted during abuse tests by overcharge of a commercial Li-ion battery,” Journal of Power Sources, Vol.389, pp.106-119 (2018)

Gioia, G. and Cuitino, A., “The energetics of heterogeneous deformation in open-cell elastic foams,” APS Meeting Abstracts, Vol.457, pp.1079-1096 (2001)

Guo, M., Sikha, G. and White, R.E., “Single-Particle Model for a Lithium-Ion Cell: Thermal Behavior,” Journal of the Electrochemical Society, Vol.158, No.2, pp.A122-A132 (2011)

Kakimoto, N. and Goto, K., “Capacity-Fading Model of Lithium-Ion Battery Applicable to Multicell Storage Systems,” IEEE Transactions on Sustainable Energy, Vol.7, No.1, pp.108-117 (2016)

Kupper, C., Spitznagel, S., Doring, H., Danzer, M.A., Gutierrez, C., Kvasha, A. and Bessler, W.G., "Combined modeling and experimental study of the high-temperature behavior of a lithium-ion cell: Differential scanning calorimetry, accelerating rate calorimetry and external short circuit,” Electrochemical Acta, Vol.306, pp.209-219 (2019)

Lagadec, M.F., Zahn, R. and Wood, V., “Characterization and performance evaluation of lithium-ion battery separators,” Nature Energy, Vol.4, pp.16-25 (2019)

Liu, C., Li, H., Kong, X. and Zhao, J., “Modeling analysis of the effect of battery design on internal short circuit hazard in LiNi0.8Co0.1Mn0.1O2/SiOx-graphite lithium-ion batteries,” International Journal of Heat and Mass Transfer, Vol.153, pp.119590 (2020)

Liu, X.T., Kan, F.C., Wang, H.J., Xin, X.F., Wang, Z.Q. and Huang, H., “Fatigue life prediction of clutch sleeve based on abrasion mathematical model in service period,” Fatigue & Fracture of Engineering Materials & Structures, Vol.43, No.3, pp.488-501 (2020)

Marques, P., Garcia, R., Kulay, L. and Freire, F., “Comparative life cycle assessment of lithium-ion batteries for electric vehicles addressing capacity fade,” Journal of Cleaner Production, Vol.229, pp.787-794 (2019)

Naseem, A., Sun, X.G., Muhammad, Y.A. and Fakhar, Z., “A gelatin-based artificial SEI for lithium deposition regulation and polysulfide shuttle suppression in lithium-sulfur batteries,” Journal of Energy Chemistry, Vol.52, pp.310-317 (2021)

Ning, G., White, R.E. and Popov, B.N., “A generalized cycle life model of rechargeable Li-ion batteries,” Electrochemica Acta, Vol.51, No.10, pp.2012-2022 (2006)

Peng, X.B., Ma, C., Garg, A., Bao, N.S. and Liao, X.P., “Thermal performance investigation of an air-cooled lithium-ion battery pack considering the inconsistency of battery cells,” Applied Thermal Engineering, Vol.153, pp.596-603 (2019)

Quan, X., Yang, D.Z., Wang, Z.L., Ren, Y., Sun, B., Qiang, F. and Qian, C., “Multiphysical modeling for life analysis of lithium-ion battery pack in electric vehicles,” Renewable and Sustainable Energy Reviews, Vol.131, pp.109993 (2020)

Ramadass, P., Haran, B., Gomadam, P.M., White, R. and Popov, B.N., “Development of first principles capacity fade model for Li-Ion cells,” Journal of the Electrochemical Society, Vol.151, pp.A196-A203 (2004)

Reichl, T. and Hrzina, P., “Capacity detection of internal short circuit,” Journal of Energy Storage, Vol.15, pp.345-349 (2018)

Sarkar, A., Shrotriya, P. and Chandra, A., “Modeling of separator failure in lithium-ion pouch cells under compression,” Journal of power sources, Vol.435, pp.225756 (2019)

Seaman, A., Dao, T.S. and Mcphee, J., “A survey of mathematics-based equivalent-circuit and electrochemical battery models for hybrid and electric vehicle simulation," Journal of Power Sources, Vol.256, pp.410-424 (2014)

Shang Z.Z., Qi, H.Z., Liu, X.T., Ouyang, C.Z. and Wang Y.S., "Structural optimization of lithium-ion battery for improving thermal performance based on a liquid cooling system," International Journal of Heat and Mass Transfer, Vol.130, pp.33-41 (2019)

Sharova, V., Moretti, A., Giffin, G.A., Carvalho, D.V. and Passerini, S, "Evaluation of carbon-coated graphite as a negative electrode material for Li-ion batteries," C-Journal of Carbon Research, Vol.3, No.3, pp.22 (2017)

Tian, J., Wang, Y. and Chen, Z., "An improved single particle model for lithium-ion batteries based on main stress factor compensation," Journal of Cleaner Production, Vol.278, pp.123456 (2021)

Tomai, T., Hyodo, H., Komatsu, D. and Honma, I., "Analysis of Degradation Mechanisms in Quinone-Based Electrodes for Aqueous Electrolyte System via In-Situ XRD Measurements," Journal of Physical Chemistry C, Vol.122, No.5, pp.2461-2466 (2018)

Wang, M.L., Liu, X.T., Wang, X.L. and Wang, Y.S., "Research on load spectrum construction of automobile key parts based on Monte Carlo Sampling," Journal of Testing and Evaluation, Vol.46, No.3, pp.1099-1110 (2018)

Weiglhofer, W.S., Lakhtakia, A. and Michel, B., "Maxwell Garnett and Bruggeman formalisms for a particulate composite with bianisotropic host medium," Microwave and Optical Technology Letters, Vol.15, pp.263-266(1997)

Weng, J., Yang, X., Zhang, G., Ouyang, D., Chen, M. and Wang, J., "Optimization of the detailed factors in a phase-change-material module for battery thermal management," International Journal of Heat and Mass Transfer, Vol.138, pp.126-134 (2019)

Yang, A., Wang, Y., Yang, F.F., Wang, D. and Zi, Y.Y., "A comprehensive investigation of lithium-ion battery degradation performance at different discharge rates," Journal of Power Sources, Vol.443, pp.227108 (2019)

Yu, X.G., Wang, X., Liu, X.T. and Wang, YS, "Reliability reallocation for cost uncertainty of fuel cell vehicles via improved differential evolution algorithm," Quality and Reliability Engineering International, Vol.36, No.1, pp.303-314 (2020)

Yusuf, A., Avvaru, V.S., Dirican, M., Sun, C.C. and Wang, D.Y., "Low heat yielding electrospun phosphenanthrene oxide loaded polyacrylonitrile composite separators for safer high energy density lithium-ion batteries," Applied Materials Today, Vol.20, pp.100675 (2020)

Zhang, A.B., Wang, B.L., Li, G.Y., Wang, J. and Du, J.K., "Fracture analysis of bi-layer electrode in lithium-ion battery caused by diffusion-induced stress," Engineering Fracture Mechanics, Vol.235, pp.107189 (2020)

Zhang, K., Zhang, Y.W., Zhou, J.W., Li, Y., Zheng, B., Yang, F. and Kai, Y., "A stress-based charging protocol for silicon anode in lithium-ion battery," Theoretical and experimental studies, Vol.32, pp.101765 (2020)

Zheng, Z.N., Gao, X. and Luo, Y.W., "Influence of copolymer chain sequence on electrode latex binder for lithium-ion batteries," Colloid and Polymer Science, Vol.297, No.10, pp.1287-1299 (2019)

Zhong, Y.T., Liu, Y.L. and Wang, B., "Stress analysis in cylindrical composition-gradient electrodes of lithium-ion battery," Ceramics International, Vol.7, pp.075115 (2017)

Zhou, Z., Zhang, J., Chen, S., Yao, H., Zhao, Y., Kuang, Q., Fan, Q. and Dong, Y., "The electrochemical performance and multielectron reaction mechanism of NiV2O6 as anovel anode material for lithium-ion batteries," Electrochimica Acta, Vol.359, pp.136979 (2020)

基於多物理場耦合的鋰離子電池容量衰減模擬

宋志昊 劉新田 錢康鋒 黃碧雄
王一全
上海工程技術大學機械與汽車工程學院

摘要

為了分析 1C 充放電條件下的電池壽命，選擇了鋰離子電池作為研究物件，基於多孔電極理論構建了電池的電化學模擬模型。利用鋰離子電池組採集的應力譜，分析了外部應力對鋰電池性能的影響。通過電化學-固體傳熱-流體散熱-外部應力耦合模擬了鋰離子電池的 1C 充放電條件，並分析了鋰電池的迴圈壽命。對固體電解質間相（SEI）生成反應採用了減少計算量的方法，分析了應力對 SEI 生成的影響。